HAL
open science

Improving the sustainability of granular iron/pumice systems for water treatment

Stafania Bilardi, Paolo S. Calabro, Sabine Caré, Nicola Moraci, Chicgoua Noubactep

To cite this version:

Stafania Bilardi, Paolo S. Calabro, Sabine Caré, Nicola Moraci, Chicgoua Noubactep. Improving the sustainability of granular iron/pumice systems for water treatment. Journal of Environmental Management, 2013, 121, pp.133-141. 10.1016/j.jenvman.2013.02.042 . hal-00809731

HAL Id: hal-00809731

https://enpc.hal.science/hal-00809731v1

Submitted on 11 Apr 2013

HAL is a multi-disciplinary open access archive for the deposit and dissemination of scientific research documents, whether they are published or not. The documents may come from teaching and research institutions in France or abroad, or from public or private research centers.

L'archive ouverte pluridisciplinaire **HAL**, est destinée au dépôt et à la diffusion de documents scientifiques de niveau recherche, publiés ou non, émanant des établissements d'enseignement et de recherche français ou étrangers, des laboratoires publics ou privés.

Improving the sustainability of granular iron/pumice systems for water treatment

Stefania Bilardi[a], Paolo S. Calabrò[a], Sabine Caré[b], Nicola Moraci[a], Chicgoua Noubactep[c,d,*]

[a]Università degli Studi Mediterranea di Reggio Calabria, MECMAT, Mechanics and Materials Department, Faculty of Engineering, Via Graziella, loc. Feo di Vito, 89122 Reggio Calabria, Italy.

[b]Université Paris-Est, Laboratoire Navier (UMR 8205), CNRS, ENPC, IFSTTAR, F-77455 Marne-la-Vallée, France;

[c]Angewandte Geologie, Universität Göttingen, Goldschmidtstraße 3, D-37077, Göttingen, Germany.

[d]Kultur und Nachhaltige Entwicklung CDD e.V., Postfach 1502, D-37005 Göttingen, Germany

* e-mail: cnoubac@gwdg.de; Tel. +49 551 39 3191, Fax. +49 551 399379.

Abstract

Metallic iron (Fe^0) is currently used in subsurface and above-ground water filtration systems on a pragmatic basis. Recent theoretical studies have indicated that, to be sustainable, such systems should not contain more than 60 % Fe^0 (vol/vol). The prediction was already validated in a Fe^0/sand system using methylene blue as an operational tracer. The present work is the first attempt to experimentally verify the new concept using pumice particles. A well-characterized pumice sample is used as operational supporting material and is mixed with 200 g of a granular Fe^0, in volumetric proportions, varying from 0 to 100 %. The resulting column systems are characterized (i) by the time dependent evolution of their hydraulic conductivity and (ii) for their efficiency for the removal of Cu^{II}, Ni^{II}, and Zn^{II} from a three-contaminants-solution (about 0.30 M of each metal). Test results showed a clear sustainability of the long term hydraulic conductivity with decreasing Fe^0/pumice ratio. In fact, the pure Fe^0 system clogged after 17 days, while the 25 % Fe^0 system could operate for 36 days. The experimental data confirmed the view that well-designed Fe^0 PRBs may be successful at removing both reducible and irreducible metal species.

* Corresponding author: Tel. +49 551 39 3191, Fax. +49 551 399379; E-mail: cnoubac@gwdg.de.

Keywords: Column study, Hydraulic conductivity, Reactive walls, Pumice, Zerovalent iron.

1 Introduction

Filter materials for water treatment are ideally used in small quantities. The high required affinity of used aggregates for efficient water treatment is not always readily available in natural materials. On the other hand, efficient filters should be designed to make the best use of these latter with the minimum of processing (Smith et al., 2001). Alternatively, readily available natural materials (e.g. anthracite, gravel, pumice, sand) may be mixed to low cost synthetic aggregates/materials (activated carbon, blast furnace slag, metallic iron) for improving the performance of the resulting water treatment systems. The key properties determining the permeability, the stability and the longevity (sustainability) of granular filters include porosity/texture of used particles, particle size, particle shape and particle size distribution or material sorting (Haarhoff and Vessal, 2010; Kubare and Haarhoff, 2010; Miyajima, 2012; Btatkeu et al., 2013; Caré et al., 2013). Two key interrelated properties required for a sustainable filter include: (i) high permeability combined with resistance to internal erosion of fines and (ii) low susceptibility to chemical attack (prerequisite 1).

Granular metallic iron (Fe^0), as currently used in water treatment, is a reactive material and its oxidative dissolution by water is a volumetric expansive process (Pilling and Bedworth, 1923; Caré et al., 2008). This means that Fe^0 is highly susceptible to chemical attack and the products of this chemical reaction are fines/precipitates (iron hydroxides and oxides). In other words, 'prerequisite 1' is not satisfied as the sustainability of Fe^0 filters is impaired by the same properties making Fe^0 an attractive material: the chemical reactivity of iron (Liu et al. 2013). However, without considering these key properties, Fe^0 permeable reactive barriers (Fe^0 PRBs) have become an established technology for the treatment of contaminated groundwater (O'Hannesin and Gillham, 1998; Li et al., 2006; Li and Benson, 2010; Comba et al., 2011; Gheju, 2011; Ruhl et al., 2012). Currently, about 180 Fe^0 PRBs have been installed worldwide (ITRC, 2011).

The fundamental mechanisms of contaminant removal in Fe^0 filtration systems are adsorption, co-precipitation and adsorptive size-exclusion (Noubactep, 2008; 2010; 2011). Contaminant removal also implies iron corrosion (Lavine et el., 2001; You et al., 2005; Jiao et al., 2009; Ghauch et al., 2011; Gheju and Balcu 2011). Therefore, due to the volumetric expansive nature of this process ('prerequisite 1'), the remediation of contaminated groundwater necessarily results in the gradual clogging of the Fe^0 PRB, and thus in the deterioration of the permeable barrier hydraulic conductivity (permeability loss) over time (Zhang and Gillham, 2005; Courcelles et al., 2011; Knowles et al., 2011; Jeen et al., 2012; Miyajima, 2012; Noubactep, 2013a).

The gradual clogging (permeability loss) of Fe^0 filtration systems has several origins: (i) biological activities like biofilm growth or biocorrosion, (ii) chemical processes like (hydr)oxide or calcite precipitation, (iii) physical processes allowing the retention of fine particles in the PRB pores, and (iv) production and accumulation of gases (mainly H_2). Pores clogging could generate a decrease in treatment performance and the bypass of untreated contaminated groundwater (Courcelles et al., 2011; Knowles et al., 2011; Jeen et al., 2012). Therefore, PRBs clogging issues will require cost-intensive reactive material substitution, if satisfactory operational performance has to be maintained. The present work is focused on the characterization of PRB clogging due to pore filling by in-situ generated iron corrosion products neglecting the other possible phenomena that could contribute to permeability reduction (i.e. gas retention, biocorrosion, biofouling) (Henderson and Demond, 2011; Caré et al., 2012; Noubactep, 2013a).

The objective of the present work is to characterize the efficiency of Fe^0/pumice granular mixtures for contaminant removal in column experiments containing 0 to 100 % Fe^0 (vol/vol). Fe^0 is admixed to a well-characterized pumice specimen (Moraci and Calabrò, 2010; Calabrò et al., 2011; Bilardi et al., 2013a), in different volumetric ratios. The model oxic solution (about 8 mg/L O_2) contained about 0.30 M of Cu^{II}, Ni^{II}, and Zn^{II}. The evolution of the systems is characterized by

determining the (i) extent of contaminant removal (or retention), and (ii) variation of hydraulic conductivity.

2 Materials and methods

2.1 Chemicals

Copper(II) nitrate hydrate (purity 99.999), nickel(II) nitrate hexahydrate (purity 99.999) and zinc(II) nitrate hexahydrate (purity 99.000) were obtained from Sigma-Aldrich. The three heavy metals are used for their different affinity to iron oxides (Wang and Qin, 2007; Moreira and Alleoni, 2010; Vodyanitskii, 2010). In addition, a survey of the electrode potential (E^0) of involved couples indicated differential redox behaviours. In fact, Zn^{II} (E^0 = -0.763 V) can not be reduced by Fe^0 (E^0 = -0.440 V) while Cu (E^0 = 0.337 V) is readily reduced. The electrode potential of Ni (E^0 = -0.250 V) is relatively close to that of Fe (ΔE^0 = 0.19 V) such that quantitative reduction can not be expected.

2.2 Solid materials

Pumice: the used pumice originates from Lipari (Aeolian Islands, Sicily – Italy); its mineralogical composition was determined as follows: SiO_2: 71.75 %; Al_2O_3: 12.33 %; K_2O: 4.47 %; Na_2O: 3.59 %; Fe_2O_3: 1.98 %; moreover it contains about 4 % of bound water (structural water) and traces of other compounds (e.g. CaO, SO_3, MgO, TiO_2, FeO, MnO, P_2O_5). Although pumice exhibited a non negligible removal capacity for heavy metals (Moraci and Calabrò, 2010; Calabrò et al., 2011), it was used here as an operational inert material with the virtual capacity of storing corrosion products in its pores and retarding clogging (Moraci and Calabrò, 2010; Noubactep and Caré, 2010; Noubactep et al. 2012a; Noubactep et al. 2012b). The material is characterized by uniform grain size distribution. The mean grain size (d_{50}) is about 0.3 mm and the coefficient of uniformity (U) is 1.4 (see Supporting Information).

Metallic iron: the used Fe^0 is of the type FERBLAST RI 850/3.5, distributed by Pometon S.p.A., Mestre - Italy. The material contents mainly iron (> 99.74 %). Identified impurities included mainly Mn (0.26 %), O, S and C. The material is characterized by uniform grain size distribution. The

mean grain size (d_{50}) is about 0.5 mm and the coefficient of uniformity (U) is 2 (see Supporting Information).

The microstructure of used Fe^0 and pumice was characterized using Mercury Intrusion Porosimetry (MIP) measurements and by Scanning Electron Microscopy (SEM) observations (see Supporting Information).

2.3 Columns experiments

The used solutions were obtained by dissolving copper nitrate, nickel nitrate and zinc nitrate in distilled water. The molar concentration of the resulting solution was as follows: 0.27 M Cu, 0.29 M Ni and 0.37 M Zn. The corresponding mass concentrations are 17 mg/L Cu, 17 mg/L Ni, and 23 mg/L Zn.

No attempt was made to control the mass of dissolved oxygen (DO) present during the column experiments. The main source of molecular oxygen is the air in the headspace of the PE bottles. It can be assumed that the model solutions contained up to 8 mg/L DO. The role of dissolved oxygen in accelerating the kinetics of aqueous iron corrosion is well-documented (e.g. Cohen, 1959; Stratmann and Müller, 1994). Using an oxic solution is a tool to enable the characterization of clogging under relevant conditions at reasonable experimental durations.

Simplified model solutions (no carbonates, bicarbonates and relevant cations) were used as this work is a seminal one focused on the impact of molecular O_2 on the clogging process of Fe^0 PRBs as influenced by pumice addition in various proportions. Testing more complex solutions relevant to simulate natural situation could be built on the results from these simplified systems.

Laboratory scale polymethyl methacrylate (Plexiglas) columns were operated in up-flow mode. The influent solution was pumped upwards from a single PE bottle using a precision peristaltic pump (Ismatec, ISM930). In all the tests the flow rate was maintained constant at a value of 0.5 mL/min. Tygon tubes were used to connect inlet reservoir, pump, columns and outlet. Six plexiglas columns (50 cm long, 5.0 cm inner diameter) were used in the experiments (Fig. 1).

The ratio column diameter (D) to average material particle size (d) ensured the prevention of channelling and wall effects. In fact, used D/d ratio (actually 100 to 165) is by far larger than the threshold value of 50 (Badruzzaman and Westerhoff, 2005).

Six different systems were investigated (Systems A through F) (Tab. 1). System A was the operational reference system containing only pumice (0 % Fe^0) and system F was a pure iron column (100 % Fe^0). The volumetric proportion of Fe^0 in the 4 other systems was 10, 25, 50 and 75 % following a procedure recently presented (Noubactep and Caré, 2011; Noubactep et al. 2012b). In systems B to F, the mass of iron was fixed to 200 g. This mass represented either 100 % of the reactive zone (rz) or the relevant volumetric proportion of rz (Fig. 1, Tab. 1). Tab. 1 summarizes the theoretical ($rz_{theor;}$ i.e. the height of the column occupied by the reactive medium if Fe^0 and pumice were used in series and not as a mixture) and measured (rz_{eff} i.e. the height of the reactive zone in the column effectively measured) reactive zone for each individual systems.

The hydraulic conductivity was determined during the column tests, by either constant-head ($k > 10^{-6}$ m/s) or variable-head ($k < 10^{-6}$ m/s) permeability methods (Head and Keeton, 2008), at given times to assess the permeability of the systems. During hydraulic conductivity determinations, the test was interrupted and a tank or a burette, filled with the same contaminated solution used during the test, was connected to the column in order to carry out the appropriate procedure. At the end of the permeability test the flow in the column was re-established with the operation mode illustrated before. The duration of these procedures was very limited therefore the disturbance to the test was fully acceptable. The column tests were performed at room temperature (21 ± 4 °C). Solution specimens for analysis were collected from the columns outlet at periodic intervals and the experiments where prolonged until contaminant breakthrough (system A) or a significant loss of the hydraulic conductivity (systems C to F) was observed; only system B was voluntarily stopped after 90 days. Tab. SI summarizes the experimental research program (Supporting Information).

The aqueous concentrations of Cu, Ni and Zn were determined by Atomic Absorption Spectrophotometry (AAS - Shimadzu AA – 6701F) using conventional Standard Methods (APHA 2005).

2.4 Expression of the experimental results

In order to characterize the magnitude of tested systems for contaminant removal, the removal efficiency (E) and the specific removal (E_s) were calculated using Eq. 1 and Eq. 2 (Moraci and Calabrò, 2010; Btatkeu et al., 2013).

$$E = m_{rem}/m_{in}*100 \quad (1)$$

$$E_s = m_{rem}/m_{Fe}*100 \quad (2)$$

where m_{in} is the mass of contaminant flowed into the column, m_{rem} is the mass of removed contaminant, and m_{Fe} the mass of Fe^0 present in the column.

3 Results and discussion

3.1 Contaminant removal

The presentation is based on the concept that tested contaminants are removed in Fe^0 columns (at pH > 5) by adsorption, co-precipitation and adsorptive size-exclusion (Noubactep, 2008; 2010; 2011). Given the importance of the pH value for this concept, the results of pH monitoring are presented first.

3.1.1 pH value

Figure 2 summarizes the results of the evolution of the pH value in all investigated systems. It is shown that in the reference system (100 % pumice), the initial pH (6.3) decreased to 5.8 and remained constant for the entire column tests duration. The slight pH decrease could be attributed to acidic sites at the pumice surface (Eq. 3). In all other systems, the pH value first increased to value > 9.0 and progressively decreased to values close to 6.0 – 7.0. The observed pH increase is certainly due to iron corrosion which consumes H^+ (Eq. 4).

$$SiO_{2(s)} + 2\ H_2O \Rightarrow H_4SiO_4(aq) \quad (3)$$

$$Fe^0 + 2\,H^+ \Rightarrow Fe^{2+} + H_2 \qquad (4)$$

The subsequent progressive decrease of the pH value is consistent with lowered kinetics of iron corrosion due to the formation of an oxide scale at the Fe^0 surface (Cohen, 1959; Evans, 1969; Aleksanyan et al., 2007; Nesic, 2007). The most important issue from Fig. 2 is that for all Fe^0-containing systems, the effluent pH value is higher than 5.0. This suggests that contaminant removal by adsorption, co-precipitation and adsorptive size-exclusion (Noubactep, 2011) could be quantitative within these columns.

3.1.2 Iron release

Figure 3 summarizes the results of the evolution of dissolved iron concentration in the effluent. It is evident from Fig. 3a, that the highest iron release was observed in the system with the lowest Fe^0 ratio (B, 10 % Fe^0). The lowest Fe^0 ratio corresponds to the highest amount of pumice (243 g - Tab. 1), acidifying the system after Eq. 3. The transport of iron corrosion products is certainly favoured at low pH values and may be favoured by larger porosity (Nimmo, 2004; Woudberg and Du Plessis, 2008; Glover and Walker, 2009). In other words, in all other systems, even more iron could be dissolved but it is retained within the system by (i) adsorption onto available iron oxides or onto pumice, or (ii) precipitation as iron (hydr)oxides (Miyajima, 2012; Miyajima and Noubactep, 2013). It is very important to notice that the extent of iron release depends primarily on the intrinsic reactivity of used Fe^0. Although data on iron release from column experiments are available in the literature (e.g. Westerhoff and James, 2003) it is impossible to make a quantitative comparison. In fact, a parameter (or an index) to characterize the intrinsic reactivity of Fe^0 is still lacking (Noubactep et al., 2009; Noubactep, 2012).

Fig. 3b shows that, apart from system B (10:90), in all other systems less than 1 mg/L iron was released in the effluent solution. It is interesting to note that, for the remaining systems, the two columns with the largest proportion of Fe^0 (50 and 100 %) exhibited the highest iron release.

3.1.3 Metal concentration

Table 2 summarizes the results of the removal of Cu^{II}, Ni^{II} and Zn^{II} in terms of removal efficiency E, and of specific removal efficiency E_s for all the 5 systems containing Fe^0. While, reading this table, it should be kept in mind that the experimental duration was variable as most of the experiments were stopped because of significant permeability loss (see Tab. 1). Nevertheless, it can be seen that 367 to 2881 mg of individual contaminants flowed into the columns and were retained with an efficiency E > 90.0 %. Moreover, the specific efficiency (E_s) varied from 1.7 to 13.6 mg contaminant per g of Fe^0.

An important feature from Tab. 2 regards the suitability of E_s values (Eq. 2) for the characterization of processes occurring in Fe^0/H_2O systems (Btatkeu et al., 2013; Miyajima and Noubactep, 2013). Normalizing the extent of contaminant removal (m_{rev} - Eq. 2) by the available amount of Fe^0 (here 200 g) is only valid, if there is a clear linear relationship between iron corrosion and contaminant removal. Such a relationship has not been demonstrated in the Fe^0 remediation literature despite repeated reports on reaction orders. Moreover, an adequate argumentation for adsorptive processes has been simply transposed to systems, where adsorption is only one (and not necessarily the dominant) removal path.

In pure adsorption systems (e.g. activated carbon, iron oxide, clay), the whole mass of adsorbing material is present at the start of the removal process (t_0 or t = 0), its adsorption capacity can be exhausted with the time. In a Fe^0 system on the contrary, adsorbing species are generated in situ after the start of the experiment ($t > t_0$). Accordingly the extent of contaminant removal depends on the kinetics of iron corrosion and the affinity of contaminants for corrosion products as far as pure adsorption is concerned. Additionally, contaminants are also removed by co-precipitation and size-exclusion. In other words, normalizing the extent of contaminant removal by the Fe^0 amount requires at least the knowledge of the intrinsic reactivity of used Fe^0 and the impact of operational parameters thereon. The most relevant operational parameter in the present work is the volumetric Fe^0:pumice ratio.

Figure 4 shows that the influence of the volumetric Fe^0:pumice ratio on the removal efficiency of Cu^{2+}, Ni^{2+}, Zn^{2+} is very similar to the influence of the adsorbent amount on adsorption of Mn^{2+} by clay minerals (Goldani et al., 2013). These authors reported on a decreasing trend of the adsorption capacity (q_e value / mg g^{-1}) for Mn^{2+} with increasing adsorbent amount (50 to 500 mg). This observation was mainly rationalized by the fact that a large adsorbent amount reduces the unsaturation of the adsorption sites. Correspondingly, the number of such sites per unit mass comes down resulting in comparatively less adsorption at higher adsorbent amount. In the present work, the Fe^0 amount is constant (200 g), only its volumetric ratio in the mixture to pumice varies. Moreover, a higher Fe^0 ratio is coupled to a shorter reactive zone (e.g. 2.6 cm for 100 % Fe^0 and 26.2 cm for 10 % Fe^0). Thus, a higher Fe^0 volumetric ratio may create particle aggregation (cementation), decreasing the total number of adsorption sites, decreasing the porosity of the reactive zone, and increasing the diffusion path to adsorption sites. Altogether, these factors contribute to the decrease of the amount of contaminant adsorbed, assuming that the same amount of adsorbent is generated in all systems. As summarized in Tab. 2, except system B (10 % Fe^0), metal removal was quantitative in all other systems.

Contaminant breakthrough was observed in other systems only short before the experiment was stopped and was mainly attributed to transport through preferential flow paths (Miyajima and Noubactep, 2013a and ref. cited therein). Even under such conditions the concentration of Cu and Zn remained below 1 mg/L whereas the concentration of Ni exceeded 4 mg/L for system F (100 % Fe^0) and system D (50 % Fe^0) but not for system E (75 % Fe^0). This anomaly in the sequence D/E/F confirms that the process responsible for metal breakthrough near system clogging is probably a meta-stable one (preferential flow).

3.2.4 Mechanism of contaminant removal

The experimental data previously described has shown that contaminants are quantitatively removed in columns with volumetric Fe^0 ratio higher than 10 % until the system is almost clogged.

In the system with 10 % Fe^0, quantitative iron release is observed (Fig. 5). Quantitative iron release coincided with minimal contaminant removal (or contaminant breakthrough) as discussed above. This section further discusses the behaviour of system B (Fig. 5a).

The ionic radii of the investigated cations increase in the order $Ni^{2+} < Cu^{2+} < Zn^{2+}$. The metallic ions are removed by four different mechanisms (Herbert, 1996; Wang and Qin, 2007; Vodyanitskii, 2010): (i) co-precipitation with iron hydroxides, (ii) adsorption onto the (hydr)oxide surfaces, (iii) isomorphic substitution for Fe in the iron oxide structure, or adsorptive size-exclusion. In multi-element systems, the most common reported affinity sequence for iron oxides and soils is Cu > Zn > Ni (Moreira and Alleoni, 2010). This trend is confirmed by Fig. 5b.

Fig. 5a illustrates the fact that contaminants breakthrough occurs when increased iron release is observed. For example, no significant breakthrough was observed in system B until t=30 days although up to 8 mg/L Fe was released into the outlet solution. For t > 30 days Zn and Ni breakthrough occurs and the breakthrough magnitude is in agreement with the affinity sequence for iron oxides (Cu > Zn > Ni). Accordingly, breakthrough is first observed for less bounded Ni followed by Zn. As concerning Cu no breakthrough was observed through the end of the experiment. At first glance, this observation could be attributed to Cu^{II} cementation at the surface of Fe^0 in the column. In fact, Cu reduction to elemental Cu (Cu^0), as mentioned above, is very favourable and is used in many hydrometallurgical processes (Gros et al., 2011a; 2011b). However, because Cu removal in this study occurred at pH > 5 (section 3.2.1), the Fe^0 surface was necessarily covered by iron (hydr)oxides (Aleksanyan et al., 2007; Nesic, 2007) and was not directly accessible to Cu^{II} (Ni^{II} and Zn^{II}). More detailed discussion on the removal of metallic ions by Fe^0 in multi-elements system is given for instance by Cantrell et al.(1995), Qiu et al. (2000), Bartzas et al. (2006), Komnitsas et al. (2006; 2007) and Scott et al. (2011).

It should be recalled that in a Fe^0/H_2O system, so-called structural Fe^{II} (adsorbed Fe^{II}) is available and is, in some circumstances, a more efficient reducing agent than Fe^0 (White & Peterson, 1996).

Accordingly, Cu^{II} might be quantitatively removed within the oxide scale on iron. Even if Cu^{II} is reduced at the surface of Fe^0, it will be enmeshed within the matrix of iron oxides as corrosion proceeds. In conclusion, aqueous Cu^{II} is also permanently removed by the process of iron corrosion (enmeshment or co-precipitation). It should be also remembered that the stronger affinity of Cu^{II} for iron oxides (adsorption) is sufficient to rationalize the absence of Cu breakthrough for 90 days (Fig. 5b).

3.3 Hydraulic conductivity

The results presented in Fig. 6 clearly demonstrate that granular Fe^0/pumice mixtures are more sustainable in terms of long term permeability than the pure Fe^0 PRB for the decontamination of used model solution. Fig. 6a shows that the pure pumice systems exhibited an initial porosity of 72.6 % while the porosity of the pure Fe^0 system was 49.6 % (Tab. 1). Fig. 6b shows that the 100 % Fe^0 system was clogged after 17 days; the 25 % Fe^0 system after 37 days and the 10 % Fe^0 system was still highly permeable after 90 days. Even though the 10 % Fe^0 system was not efficient at removing Ni and Zn, such systems could be used to generate dissolved Fe for other purposes including: (i) in-situ generation of Fe for contaminant removal (Khan et al., 2000; Pokhrel and Viraraghavan, 2009) and (ii) oxygen scavenger to sink the O_2 concentrations in above-ground devices (Mackenzie et al., 1999; Noubactep and Schöner, 2010; Noubactep et al., 2010).

A fundamental feature from Fig. 6a is that it combines contaminant removal (here E_s value for Zn) and initial porosity. The initial porosity decreases linearly with increasing Fe^0 ratio. This behaviour is rationalized by the fact that a compact material (Fe^0) is admixed to a porous one (pumice). The initial pore volume will be progressively filled by in situ generated iron corrosion products (Caré et al., 2013) which adsorb and co-precipitate metal ions. Reduced pore volume increases size-exclusion efficiency while decreasing permeability. The challenge of designing hybrid Fe^0/material systems is to find out the optimal system concealing sustained permeability and efficient

contaminant removal. Fig. 6a confirms/shows unambiguously that such a system should contain as less Fe^0 (volumetric proportion) as possible (Caré et al., 2013; Miyajima and Noubactep, 2013). Considering the factor of 65 times to account for the differential kinetics of Fe^0 oxidation under oxic (8 mg/L O_2) and anoxic (0 mg/L O_2) conditions (Cohen, 1959), it can be argued that the shortest experimental duration (17 days) reported here could corresponds to about 1105 days under anoxic conditions. These are more than 3 years necessary to observe clogging under the experimental conditions of this work after 17 days. This result justifies the use of oxic conditions to investigate target processes under laboratory conditions. By performing parallel experiments with various amounts of molecular O_2 (Vidic and Suidan, 1991) a better characterization of the impact of the availability of molecular O_2 is possible. This effort is even urgently needed as Fe^0 beds have been proposed for an array of applications varying from pure anoxic (groundwater remediation) to oxic (household filter) systems.

Fig. 7 depicts the evolution of the experimental duration and the residual porosity (modelled, see below) as a function of the initial porosity of the columns containing Fe^0. The lowest porosity (49.6 %) corresponds to system F (100 % Fe^0) and the largest (70.5 %) to system B (10 % Fe^0). It is seen that the experimental duration (system sustainability) increases almost linearly with decreasing Fe^0 proportion from 100 to 25 %. From 25 to 10 % Fe^0 an abrupt increase of the experimental duration is observed. These results are qualitatively confirmed by the evolution of the residual porosity for $\eta = 6.4$ (Fig. 7a) where η is the coefficient of volumetric expansion of rust specimens (Caré et al., 2008).

The residual porosity ($\Phi(t)/\Phi_0$) is defined as the ratio of the porosity at time t $\Phi(t)$ to the initial porosity Φ_0 induced by the formation of rust leading to porosity loss according to:

$$\frac{\Phi(t)}{\Phi_0} = 1 - \frac{\Delta V}{\Phi_0 . V} \qquad (5)$$

Where $\Delta V = (\eta - 1)*V$ is the effective volumetric expansion of the initial volume V of Fe^0.

The residual porosity which, acting as an indicator of the hydraulic conductivity, is given for all systems in Fig. 7. The observed time-dependant decrease of the hydraulic conductivity is attributed to two different factors: (i) the decrease of the effective pore-size as concentric layers of iron oxides are formed on Fe^0, and (ii) the filling of pores by precipitated Fe species that escaped out of the oxide scale. Permeability loss due to in-situ generated particles is retarded when larger particle sizes are used. Accordingly, as the grain-size increases, the loss of hydraulic conductivity should follow the inverse trend. In other words, the kinetics of the occupation of the voids depends on the grain-size of used particles (effective pore-size).

Theoretically, for spherical grains of uniform size (monosized), the grain diameter will not impact initial porosity but only the void diameter. However, the total porosity generally increases with increasing sorting (grain size distribution), decreases with increasing sphericity and roundness of particles, decreases with the increasing of relative density (closer packing) (Gibb et al., 1984). All these aspects have to be considered to discuss literature results as well.

It appears from Fig. 7a that the residual porosity tends to zero ($\Phi(t)/\Phi_0 = 0$ or permeability loss) for clogged systems (% $Fe^0 \geq 25$ – clogging precedes Fe^0 depletion). For $Fe^0 < 25$ %, $\Phi(t)/\Phi_0 \neq 0$ at Fe^0 depletion in accordance with the evolution of the hydraulic conductivity and the test duration. At first glance, this observation could be misinterpreted as the confirmation of the proposed model. But under the experimental conditions, Fe^0 was not completely depleted. Accordingly, this experimental evidence rather suggests that the entrance zone of the column could have been rapidly clogged due to elevated O_2 levels (Mackenzie et al., 1999). The presence of O_2 leads to iron (hydr)oxides with higher expansion coefficient (η) implying a more rapid decrease of the residual porosity (Fig. 7b).

Fig. 7b depicts the modelled variation of the residual porosity for 3 different values of η (2.08, 3.03 and 6.4). It is seen that under ideal conditions (uniform corrosion), the sustainability of a Fe^0 filter depends on the availability of O_2. Accordingly the most sustainable systems is the one operating under conditions where Fe_3O_4 (η = 2.08) is the major iron corrosion product (anoxic conditions).

These conditions could be obtained in a second column in series with a first one acting as O_2 scavenger.

The fact that observed preservation of permeability with time is coupled with a decrease of contaminant removal efficiency suggests that for any Fe^0/additive couple, an increase of filter sustainability with decreasing Fe^0 proportion down to a threshold value (here 25 % Fe^0) would be observed.

This study has traceably demonstrated that admixing non expansive material with Fe^0 is a tool to increase permeable reactive barriers sustainability. In other words, an efficient but not sustainable system (100 % Fe^0) is transformed into an efficient and more sustainable one by admixing a certain volumetric proportion of pumice (here ≥ 75 %). The admixing material (here pumice) should necessarily be less expensive than Fe^0; thus, cost savings could be regarded as a positive side effect of increased performance.

3.4 Significance for future works

This study is a continuation of a broad-based work aiming at designing non-site-specific Fe^0 filtration systems for water treatment and environmental remediation in its third step.

The first step consisted in identifying the common underlying mechanisms for contaminant removal (Noubactep, 2007; 2008; 2010; 2011). Adsorption, co-precipitation and size-exclusion were identified as fundamental paths for water treatment in Fe^0 packed beds (Noubactep, 2011). This result belittled the importance of chemical reduction in the process of contaminant removal in Fe^0/H_2O systems and clearly demonstrated that Fe^0 is not a relevant reducing agent under environmental conditions. The strong fact that Fe^0 is the parent of all reducing species (e.g. Fe^{II}, Fe_3O_4, green rust, H/H_2) should never be misinterpreted as 'contaminant reduction coupled with electrochemical iron corrosion' (Noubactep, 2013b).

The second step consisted in writing the dimensionless equation of a Fe^0 packed beds (Noubactep and Caré, 2010; Noubactep et al., 2010; Noubactep and Caré, 2011; Noubactep et al., 2012a;

Noubactep et al., 2012b; Caré et al., 2013). It is important to notice, that the equation is based on the volumetric fraction of the packed beds available for 'storing' corrosion products (total porosity) (Noubactep and Caré, 2011). This theoretical work has shown that the volumetric ratio of Fe^0 in a granular mixture should ideally not exceed 60 %. The basics for a systematic research for non-site-specific Fe^0 filtration systems were established. In particular each Fe^0 material should be characterized for its intrinsic reactivity; all used materials should be characterized for their form, homogeneity and shape (Crane and Noubactep, 2012; Noubactep et al., 2012a; Caré et al., 2013).

The current third step consists in validation the equation of the column (Calabrò et al., 2011; Biliardi et al., 2013a; Biliardi et al., 2013b). In this effort methylene blue (MB) was positively tested as an operational tracer (Miyajima, 2012; Btatkeu et al., 2013; Miyajima and Noubactep, 2013). Experiments with MB confirmed theoretical predictions that a pure Fe^0 bed is not sustainable. Moreover, it could be shown that the optimal volumetric Fe^0 ratio for sustainable filters is lower 50 %. Given the large density difference between Fe^0 (7.8 g cm^3) and commonly tested additives (e.g. anthracite, gravel, pumice, sand) (< 3.0 g cm^3), this results clearly shows that the commonly used 1:1 weight ratio is not optimal as well. Experiments with MB suggested that the optimal Fe^0 volumetric ratio in a dual Fe^0/sand system is comprised between 30 and 50 %.

The present work has systematically tested the Fe^0/pumice system for the first time using Cu, Ni and Zn as model contaminants. The results showed that the optimal Fe^0 ratio for a sustainable filter is 25 %. This result could be regarded as close to 30 % as determined by Miyajima and Noubactep (2013). However, under their experimental conditions, these authors could not experimentally document permeability loss. Accordingly, the present work has provided the most reliable optimal Fe^0 ratio for sustainable Fe^0 filtration systems. In other words, this work provide the following rule of thumb for further research (including pilot plant studies): "mix one volume of Fe^0 and 3 volumes of the additive(s)". The universal validity of this rule of thumb relies on the evidence that it is based on a dimensionless equation. Thus, if a filter has to contain 1 kg Fe^0, the volume occupied by this

Fe^0 mass is used as unit and three units volume of the additives of comparable size (and shape) are to be added and homogenized.

4. Concluding remarks

Environmental remediation and water treatment using metallic iron (Fe^0) in packed beds is an established technology. Despite two decades of active research, this technology is still mostly regarded as an innovative one or has been simply declared a developed one. However, a developed technology is a technology that has established the scientific basis of the involved processes. This work has clearly confirmed theoretical predictions that: (i) pure Fe^0 beds are not sustainable as a rule, (ii) a bed made up of 25 % Fe^0 (vol/vol) and 75 % pumice is probably the most efficient system concealing sustained permeability and increased efficiency for contaminant removal, (iii) the specificity of contaminant removal in Fe^0 filters fundamentally depends on the adsorptive affinity to iron oxides (and not on the redox affinity).

The knowledge that the most sustainable filter is made up of more than 70 % (vol/vol) of pumice corroborates the view that sustainable Fe^0/aggregate filters are Fe^0-amended aggregate filters (e.g. Fe^0-amended pumice filter or Fe^0-amended sand filter). Most common natural aggregates are anthracite, sand, gravel, pumice or crushed rock. However, manufactured aggregates (e.g. blast furnace slag) can also be used as well. Basically there is an infinite number of Fe^0-amended filters as relevant aggregates may include activated carbon and biomaterial (e.g. wood and coconut shell). A Fe^0-amended filter can be regarded as a size-exclusion system in which size exclusion is improved by in situ generated iron corrosion products. This is a typical case of self-filtration. The challenge for future works is the proper design of these filters.

Further research at laboratory scale is needed to develop methodologies for the Fe^0 filter design. This effort should be accompanied by numerical modelling. Pilot scale installations are needed afterwards to fine tune determine the practicality of several aspects optimised at lab scale.

Acknowledgements

The authors are grateful to Dott Giuseppe Panzera for its essential assistance during this research activity and to the director and officials of the environmental protection sector of the province of Reggio Calabria for authorisation to use their atomic absorption spectrophotometer. SEM observations were performed at laboratory LMT Cachan, ENS de Cachan / CNRS / Université Pierre et Marie Curie (Paris 6), France. The manuscript was improved by the insightful comments of anonymous reviewers from Journal of Environmental Management.

References

Aleksanyan A.Y., Podobaev A.N., Reformatskaya I.I., 2007. Steady-state anodic dissolution of iron in neutral and close-to-neutral media. Protection of Metals 43, 66–69.

APHA, AWWA, WEF, 2005. Standard Methods for the examination of water and wastewater, 21st ed. American Public Health Association, Washington D.C. (USA).

Badruzzaman M., Westerhoff P., 2005. The application of rapid small-scale column tests in iron-based packed bed arsenic treatment systems, ACS Symposium Series, 915 (Advances in Arsenic Research): 268-283.

Bartzas G., Komnitsas K., 2010. Solid phase studies and geochemical modelling of low-cost permeable reactive barriers. J. Hazard. Mater. 183, 301–308.

Bartzas G., Komnitsas K., Paspaliaris I., 2006. Laboratory evaluation of Fe^0 barriers to treat acidic leachates. Miner. Eng. 19, 505–514.

Bilardi S., Calabrò P.S., Caré S., Moraci N., Noubactep C., 2013a. Effect of pumice and sand on the sustainability of granular iron beds for the removal of Cu^{II}, Ni^{II}, and Zn^{II}. Clean – Soil, Air, Water, doi: 10.1002/clen.201100472.

Bilardi S., Amos R.T., Blowes D.W., Calabrò P.S., Moraci N., 2013b. Reactive Transport Modeling of ZVI Column Experiments for Nickel Remediation. Ground Water Monit. Remed., doi: 10.1111/j.1745-6592.2012.01417.x.

Btatkeu K. B.D., Miyajima K., Noubactep C., Caré S., 2013. Testing the suitability of metallic iron for environmental remediation: Discoloration of methylene blue in column studies. Chem. Eng. J. 215-216, 959–968.

Calabrò P.S., Moraci N., Suraci P., 2011. Estimate of the optimum weight ratio in zero-valent iron/pumice granular mixtures used in permeable reactive barriers for the remediation of nickel contaminated groundwater. J. Hazard. Mater. 207–208, 111–116.

Cantrell K.J., Kaplan D.I., Wietsma T.W., 1995. Zero-valent iron for the in situ remediation of selected metals in groundwater. J. Hazard. Mater. 42, 201–212.

Caré S., Crane R., Calabro P.S., Ghauch A., Temgoua E., Noubactep C., 2012. Modelling the permeability loss of metallic iron water filtration systems. Clean – Soil, Air, Water, doi: 10.1002/clen.201200167.

Caré S., Nguyen Q.T., L'Hostis V., Berthaud Y., 2008. Mechanical properties of the rust layer induced by impressed current method in reinforced mortar. Cement Concrete Res. 38, 1079–1091.

Cohen M., 1959. The formation and properties of passive films on iron. Can. J. Chem. 37, 286–291.

Comba S., Di Molfetta A., Sethi R., 2011. A Comparison between field applications of nano-, micro-, and millimetric zero-valent iron for the remediation of contaminated aquifers. Water Air Soil Pollut. 215, 595–607.

Courcelles B., Modaressi-Farahmand-Razavi A., Gouvenot A., Esnault-Filet A., 2011. Influence of precipitates on hydraulic performance of permeable reactive barrier filters. Int. J. Geomech. 11, 142–151.

Evans U.R., 1969. Mechanism of rusting. Corros. Sci. 9, 813–821.

Ghauch A., Abou Assi H., Baydoun H., Tuqan A.M., Bejjani A., 2011. Fe^0-based trimetallic systems for the removal of aqueous diclofenac: Mechanism and kinetics. Chem. Eng. J. 172, 1033–1044.

Gheju M., 2011. Hexavalent chromium reduction with zero-valent iron (ZVI) in aquatic systems. Water Air Soil Pollut. 222, 103–148.

Gheju M., Balcu I., 2011. Removal of chromium from Cr(VI) polluted wastewaters by reduction with scrap iron and subsequent precipitation of resulted cations. J. Hazard. Mater. 196, 131–138.

Gibb J.P., Barcelona M.J., Ritchey J.D., LeFaivre M.H., 1984. Effective porosity of geologic materials: first annual report. Champaign, Ill; Illinois State Water Survey. SWS contract report 351.

Glover P.W.J., Walker E., 2009. Grain-size to effective pore-size transformation derived from electrokinetic theory. Geophysics 74, E17–E29.

Goldani E., Moro C.C., Maia S.M., 2013. A study employing differents clays for Fe and Mn removal in the treatment of acid mine drainage. Water Air Soil Pollut. 224, doi : 10.1007/s11270-012-1401-4.

Gros F., Baup S., Aurousseau M., 2011. Copper cementation on zinc and iron mixtures: Part 2: Fluidized bed configuration. Hydrometallurgy 106, 119–126.

Gros F., Baup S., Aurousseau M., 2011. Copper cementation on zinc and iron mixtures: Part 1: Results on rotating disc electrode. Hydrometallurgy 106, 127–133.

Haarhoff J., Vessal A., 2010. A falling-head procedure for the measurement of filter media sphericity. Water SA 36, 97–104.

Head K.H., Keeton G.P., 2008. Permeability, shear strength & compressibility tests, In: Manual of Soil Laboratory Testing, vol. 2. Whittles Publishing: United Kingdom.

Henderson A.D., Demond A.H., 2011. Impact of solids formation and gas production on the permeability of ZVI PRBs. J. Environ. Eng. 137, 689–696.

Herbert R.B., 1996. Metal retention by iron oxide precipitation from acidic ground water in Dalarna, Sweden. Appl. Geochem. 11, 229–235.

ITRC (Interstate Technology & Regulatory Council). 2011. Permeable reactive barrier: Technology update. PRB-5. Washington, D.C.: Interstate Technology & Regulatory Council, PRB: Technology Update Team. www.itrcweb.org (access: 12.12.2012).

Jeen S.-W., Amos R.T., Blowes D.W., 2012. Modeling gas formation and mineral precipitation in a granular iron column. Environ. Sci. Technol. 46, 6742–6749.

Jiao Y., Qiu C., Huang L., Wu K., Ma H., Chen S., Ma L., Wu L., 2009. Reductive dechlorination of carbon tetrachloride by zero-valent iron and related iron corrosion. Appl. Catal. B: Environ. 91, 434–440.

Khan A.H., Rasul S.B., Munir A.K.M., Habibuddowla M., Alauddin M., Newaz S.S., Hussam A., 2000. Appraisal of a simple arsenic removal method for groundwater of Bangladesh. J. Environ. Sci. Health A 35, 1021–1041.

Knowles P., Dotro G., Nivala J., García J., 2011. Clogging in subsurface-flow treatment wetlands: Occurrence and contributing factors. Ecol. Eng. 37, 99–112.

Komnitsas K., Bartzas G., Fytas K., Paspaliaris I., 2007. Long-term efficiency and kinetic evaluation of ZVI barriers during clean-up of copper containing solutions. Miner. Eng. 20, 1200–1209.

Komnitsas K., Bartzas G., Paspaliaris I., 2006. Inorganic contaminant fate assessment in zero-valent iron treatment walls. Environ. Forensics 7, 207–217.

Kubare M., Haarhoff J., 2010. Rational design of domestic biosand filters. J. Water Supply: Res. Technol. – AQUA 59 (1), 1–15.

Lavine B.K., Auslander G., Ritter J., 2001. Polarographic studies of zero valent iron as a reductant for remediation of nitroaromatics in the environment. Microchem. J. 70, 69–83.

Li L., Benson C.H., Lawson E.M., 2006. Modeling porosity reductions caused by mineral fouling in continuous-wall permeable reactive barriers. J. Contam. Hydrol. 83, 89–121.

Li L., Benson C.H., 2010. Evaluation of five strategies to limit the impact of fouling in permeable reactive barriers. J. Hazard. Mater. 181, 170–180.

Liu H., Wang Q., Wang C., Li X.-z., 2013. Electron efficiency of zero-valent iron for groundwater remediation and wastewater treatment. Chem. Eng. J. 215–216, 90–95.

Mackenzie P.D., Horney D.P., Sivavec T.M., 1999. Mineral precipitation and porosity losses in granular iron columns. J. Hazard. Mater. 68, 1–17.

Miyajima K., 2012. Optimizing the design of metallic iron filters for water treatment. Freiberg Online Geoscience 32, 60 pp.

Miyajima K., Noubactep C., 2012. Impact of Fe^0 amendment on methylene blue discoloration by sand columns. Chem. Eng. J. 217, 310–319.

Moraci N., Calabrò P.S., 2010. Heavy metals removal and hydraulic performance in zero-valent iron/pumice permeable reactive barriers. J. Environ. Manage. 91, 2336–2341.

Moreira C.S., Alleoni L.R.F., 2010. Adsorption of Cd, Cu, Ni and Zn in tropical soils under competitive and non-competitive systems. Sci. Agric. 67, 301–307.

Nesic S., 2007. Key issues related to modelling of internal corrosion of oil and gas pipelines – A review. Corros. Sci. 49, 4308–4338.

Nimmo JR. Porosity and pore size distribution. in Hillel D, editor. *Encyclopedia of Soils in the Environment*: London, Elsevier; 2004; 3:295–303.

Noubactep C., 2007. Processes of contaminant removal in "Fe^0–H_2O" systems revisited. The importance of co-precipitation. Open Environ. J. 1, 9–13.

Noubactep C., 2008. A critical review on the mechanism of contaminant removal in Fe^0–H_2O systems. Environ. Technol. 29, 909–920.

Noubactep C., Licha T., Scott T.B., Fall M., Sauter M., 2009. Exploring the influence of operational parameters on the reactivity of elemental iron materials. J. Hazard. Mater. 172, 943–951.

Noubactep C., 2010. The fundamental mechanism of aqueous contaminant removal by metallic iron. Water SA 36, 663–670.

Noubactep C., Caré S., 2010. Enhancing sustainability of household water filters by mixing metallic iron with porous materials. Chem. Eng. J. 162. 635–642.

Noubactep C., Caré S., Togue-Kamga F., Schöner A., Woafo P., 2010. Extending service life of household water filters by mixing metallic iron with sand. Clean – Soil Air Water 38, 951–959.

Noubactep C., Schöner A., 2010. Metallic iron: dawn of a new era of drinking water treatment research? Fresen. Environ. Bull. 19, 1661–1668.

Noubactep C., 2011. Aqueous contaminant removal by metallic iron: Is the paradigm shifting? Water SA 37, 419–426.

Noubactep C., Caré S., 2011. Designing laboratory metallic iron columns for better result comparability. J. Hazard. Mater. 189, 809–813.

Noubactep C., 2012. Characterizing the reactivity of metallic iron in Fe^0/As-rock/H_2O systems by long-term column experiments. Water SA. 38, 511–517.

Noubactep C., Caré S., Crane R.A., 2012a. Nanoscale metallic iron for environmental remediation: prospects and limitations. Water Air Soil Pollut. 223, 1363–1382.

Noubactep C., Temgoua E., Rahman M.A., 2012b. Designing iron-amended biosand filters for decentralized safe drinking water provision. Clean: Soil, Air, Water 40, 798–807.

Noubactep C., 2013a. On the suitability of admixing sand to metallic iron for water treatment. Int. J. Environ. Pollut. Solutions 1, 22–36.

Noubactep C., 2013b. Relevant reducing agents in remediation Fe^0/H_2O systems. Clean: Soil, Air, Water, doi:10.1002/clen.201200406.

O'Hannesin S.F., Gillham R.W., 1998. Long-term performance of an in situ "iron wall" for remediation of VOCs. Ground Water 36, 164–170.

Pilling N. B., Bedworth R.E., 1923. The oxidation of metals at high temperatures. J. Inst. Met. 29, 529–591.

Pokhrel D., Viraraghavan T., 2009. Biological filtration for removal of arsenic from drinking water. J. Environ. Manage. 90, 1956–1961.

Qiu S.R., Lai H.-F., Roberson M.J., Hunt M.L., Amrhein C., Giancarlo L.C., Flynn G.W., Yarmoff. 2000. Removal of contaminants from aqueous solution by reaction with iron surfaces. Langmuir 16, 2230–2236.

Ruhl A.S., Ünal N., Jekel M., 2012. Evaluation of two-component Fe(0) fixed bed filters with porous materials for reductive dechlorination. Chem. Eng. J. 209, 401–406.

Scott T.B., Popescu I.C., Crane R.A., Noubactep C., 2011. Nano-scale metallic iron for the treatment of solutions containing multiple inorganic contaminants. J. Hazard. Mater. 186, 280–287.

Smith M.R., Collis L., Fookes P.G., Lay J., Sims I., Smith M.R., West G., 2001. Aggregates for use in filter media. Geological Society, London, Engineering Geology Special Publications 17, 291–298.

Stratmann M., Müller J., 1994. The mechanism of the oxygen reduction on rust-covered metal substrates. Corros. Sci. 36, 327–359.

Vidic R.D., Suidan M.T., 1991. Role of dissolved oxygen on the adsorptive capacity of activated carbon for synthetic and natural organic matter. Environ. Sci. Technol. 25, 1612–1618.

Vodyanitskii Y.N., 2010. The role of iron in the fixation of heavy metals and metalloids in soils: a review of publications. Eurasian Soil Sci. 43, 519 –532.

Wang X.S., Qin Y., 2007. Relationships between heavy metals and iron oxides, fulvic acids, particle size fractions in urban roadside soils. Environ. Geol. 52, 63–69.

Westerhoff P., James J., 2003. Nitrate removal in zero-valent iron packed columns. Water Res. 37, 1818–1830.

White A.F., Peterson M.L., 1996. Reduction of aqueous transition metal species on the surfaces of Fe(II)-containing oxides. Geochim. Cosmochim. Acta 60, 3799–3814.

Woudberg S., Du Plessis J.P., 2008. Predicting the permeability of very low porosity sandstones. Transp. Porous Med. 73, 39–55.

You Y., Han J., Chiu P.C., Jin Y., 2005. Removal and inactivation of waterborne viruses using zerovalent iron. Environ. Sci. Technol. 39, 9263–9269.

Zhang Y., Gillham R.W., 2005. Effects of gas generation and precipitates on performance of Fe^0 PRBs. Ground Water 43, 113–121.

Table 1: Main characteristics of the studied columns. "Volume" is the apparent volume of granular medium. "rz_{theor}" is sum of the volumes occupied by the two media separately. "rz_{eff}" is the measured reactive zone. The estimated porosity and the duration of the experiment are also given.

System	**Volume**		**Mass**		**Column**			
	Fe^0 (%)	**Pumice** (%)	**Fe^0** (g)	**Pumice** (g)	**rz_{theor}** (cm)	**$rz_{eff.}$** (cm)	**Porosity*** (%)	**Duration** (day)
A	0	100	0.0	269.7	29.69	30.0	72.6	45
B	10	90	200.0	242.7	26.72	26.2	70.5	90
C	25	75	200.0	80.9	10.48	9.8	64.9	36**
D	50	50	200.0	27.0	5.24	5.0	59.5	28**
E	75	25	200.0	9.0	3.49	3.4	54.8	22**
F	100	0	200.0	0.0	2.62	2.6	49.6	17**

* in this values the internal porosity of the pumice is also included

** stopped because of excessive permeability loss

Table 2: Magnitude of contaminant removal in investigated systems. m_{in} is the mass of contaminant flowed into the column, E is the removal efficiency and E_s the specific removal.

System	**m_{in}**			**E**			**Es**		
	Ni	Cu	Zn	Ni	Cu	Zn	Ni	Cu	Zn
	(mg)			(%)			(mg/g)		
B	2130	2130	2881	90.1	99.8	94.2	9.58	10.6	13.6
C	881.3	881.3	1192	98.7	99.9	99.9	4.53	4.40	5.96
D	612	612	828	93.3	99.9	99.6	2.86	3.06	4.12
E	514.1	514.1	695.5	97.9	99.9	99.9	2.52	2.57	3.47
F	367.2	367.2	496.8	94.7	99.9	99.8	1.74	1.83	2.48

Figure 1

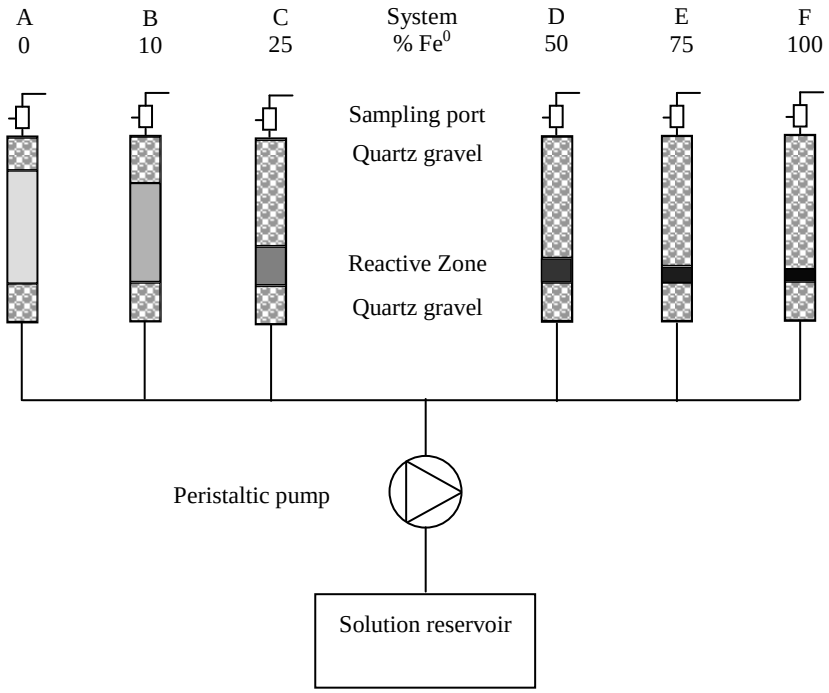
A
0
B
10
C
25
System
% Fe0
D
50
E
75
F
100
Sampling port
Quartz gravel
Reactive Zone
Quartz gravel
Peristaltic pump
Solution reservoir

Figure 2

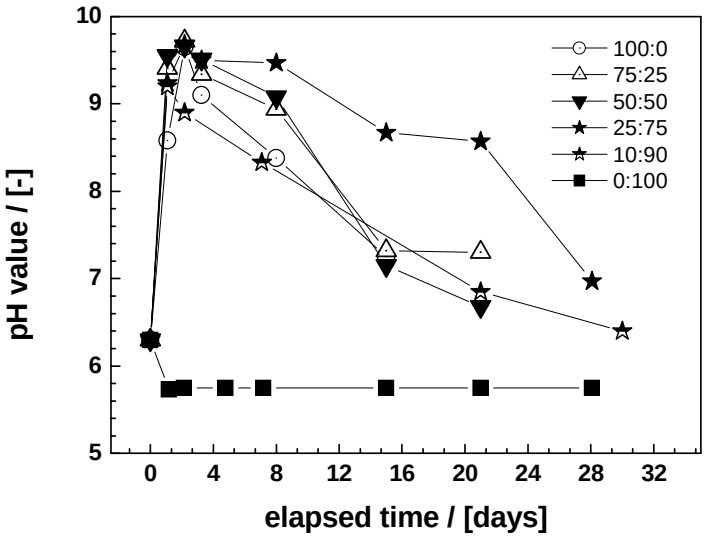
10
9
8
7
6
5
pH value / [-]
0
4
8
12
16
20
24
28
32
elapsed time / [days]
100:0
75:25
50:50
25:75
10:90
0:100

Figure 3

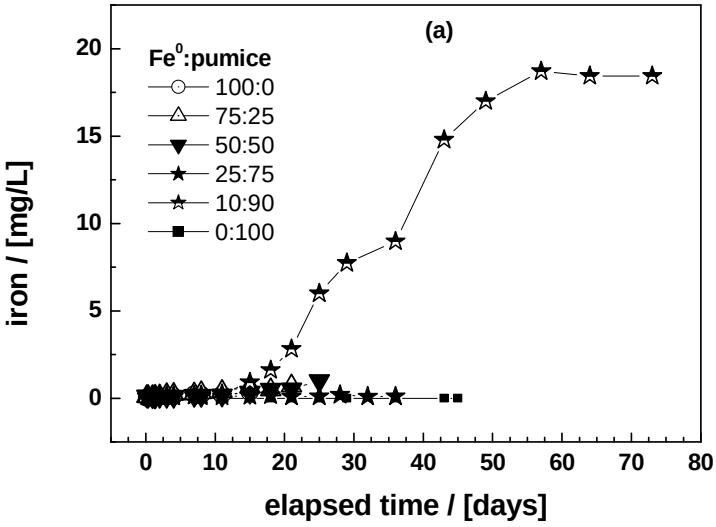
(a)
Fe0:pumice
100:0
75:25
50:50
25:75
10:90
0:100
iron / [mg/L]
elapsed time / [days]
0
5
10
15
20
0
10
20
30
40
50
60
70
80

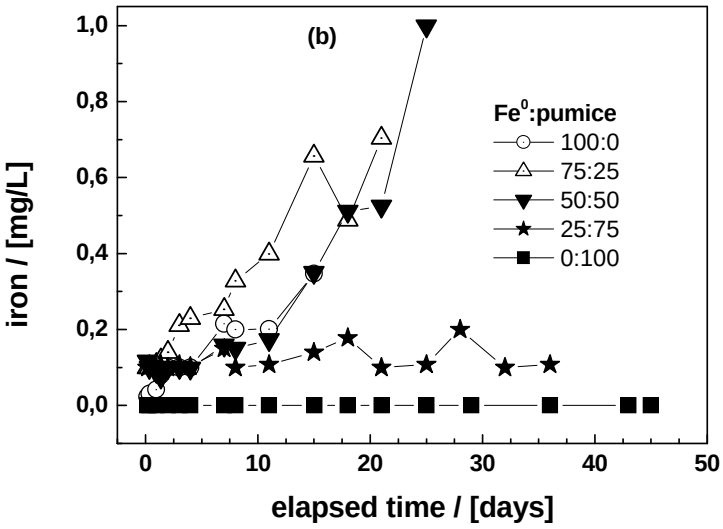
(b)
Fe0:pumice
100:0
75:25
50:50
25:75
0:100
iron / [mg/L]
elapsed time / [days]
0,0
0,2
0,4
0,6
0,8
1,0
0
10
20
30
40
50

Figure 4

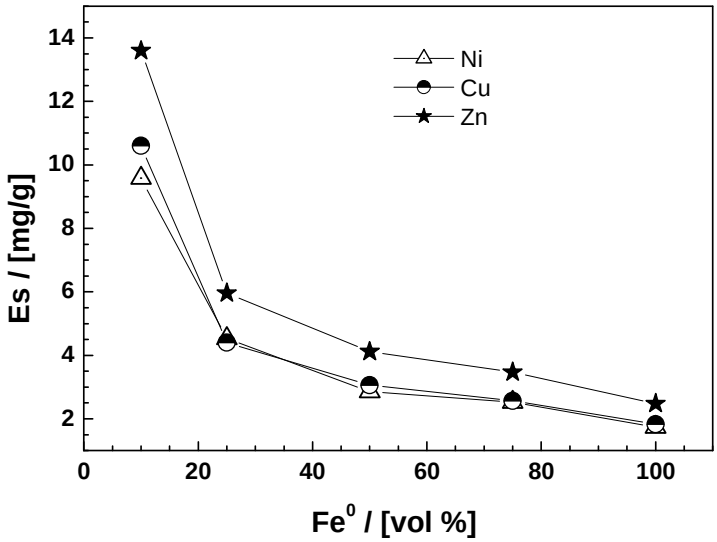

Figure 5

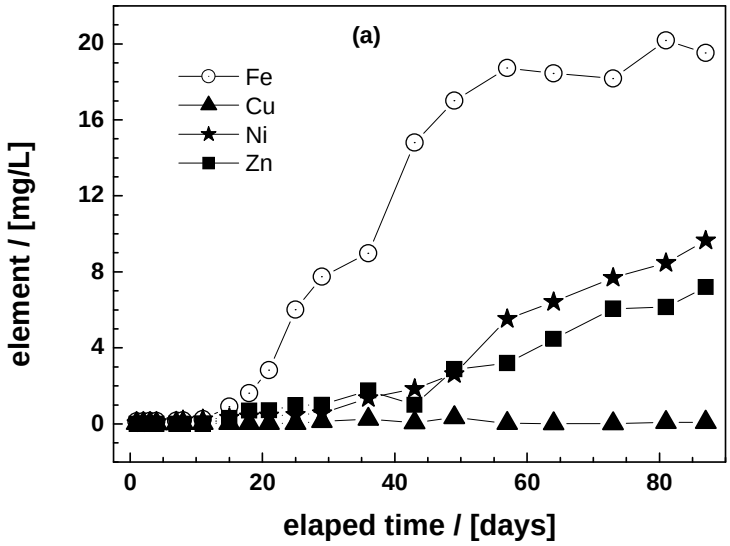
(a)
Fe
Cu
Ni
Zn
element / [mg/L]
elaped time / [days]
0
4
8
12
16
20
0
20
40
60
80

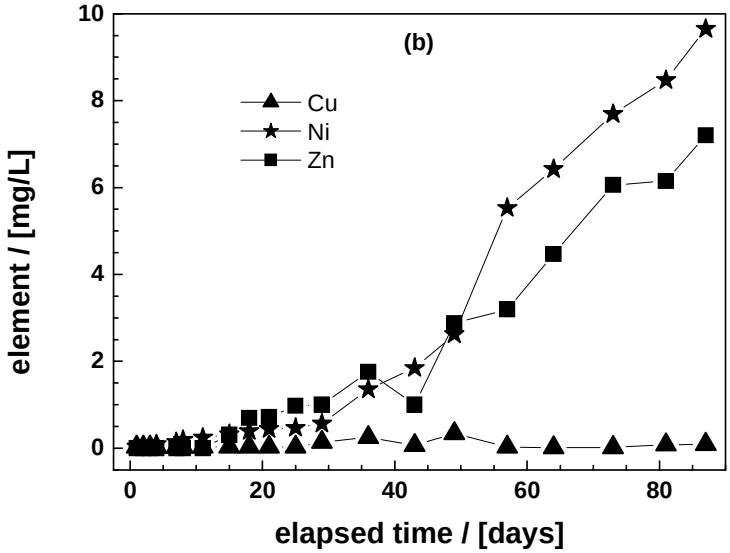
(b)
Cu
Ni
Zn
element / [mg/L]
elapsed time / [days]
0
2
4
6
8
10
0
20
40
60
80

Figure 6

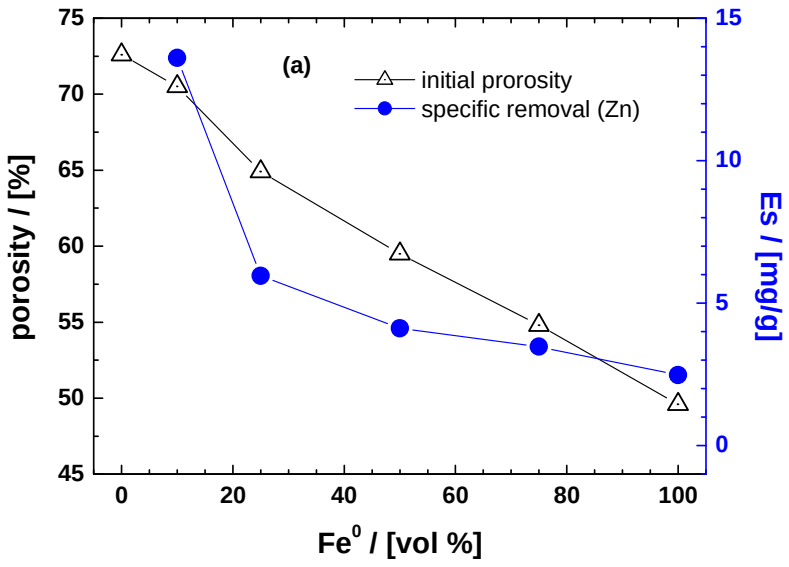
(a)
initial prorosity
specific removal (Zn)
porosity / [%]
Es / [mg/g]
Fe0 / [vol %]
75
70
65
60
55
50
45
15
10
5
0
0
20
40
60
80
100

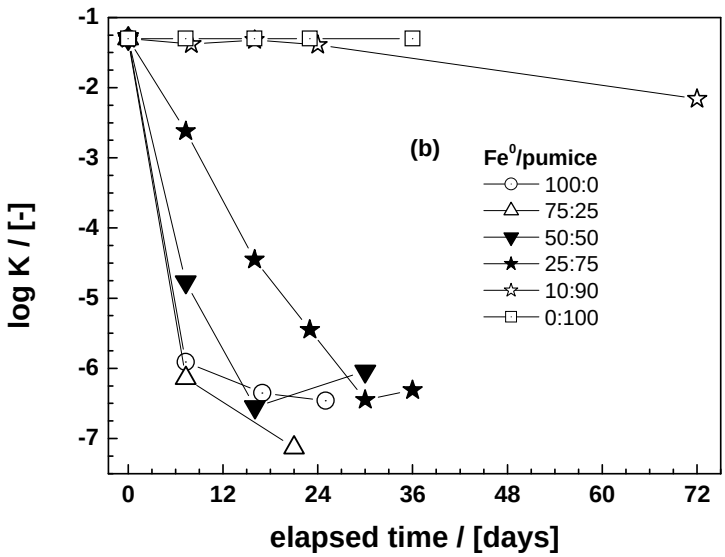
(b)
Fe0/pumice
100:0
75:25
50:50
25:75
10:90
0:100
log K / [-]
elapsed time / [days]
-1
-2
-3
-4
-5
-6
-7
0
12
24
36
48
60
72

Figure 7

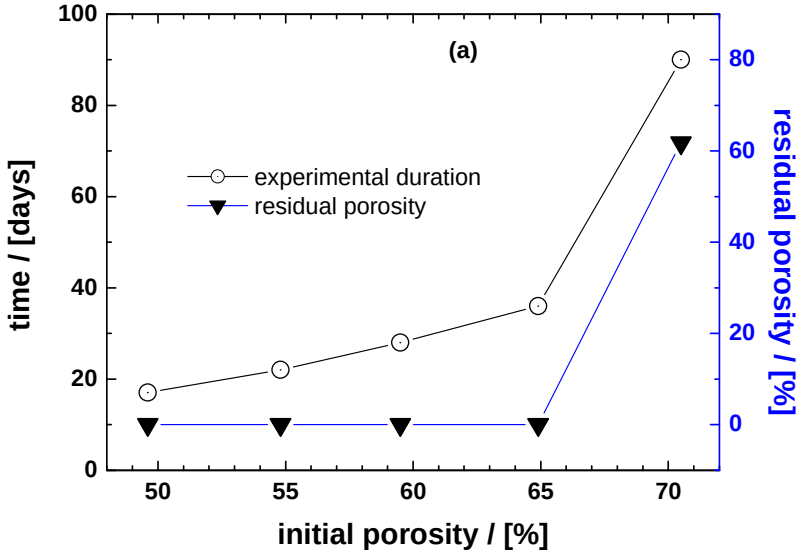
(a)
experimental duration
residual porosity
time / [days]
residual porosity / [%]
initial porosity / [%]
0
20
40
60
80
100
50
55
60
65
70

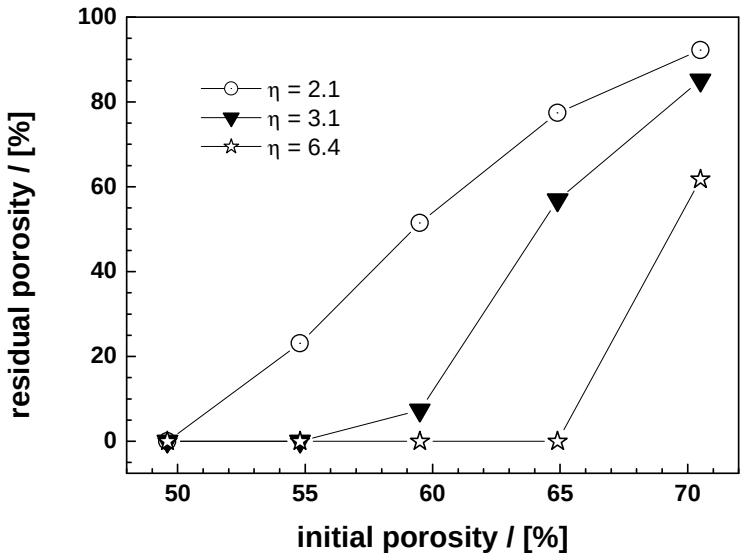
η = 2.1
η = 3.1
η = 6.4
residual porosity / [%]
initial porosity / [%]
0
20
40
60
80
100
50
55
60
65
70

Figure captions

Figure 1: Schematic diagram of the experimental design. Used materials were (i) Fe^0 (0 or 200 g), (ii) pumice (0 to 270 g), and (iii) quartz gravel (10 cm at the inlet and balance to fill the column at the outlet).

Figure 2: Time-dependant evolution of the pH value of column effluent. The lines are not fitting functions, they simply connect points to facilitate visualization.

Figure 3: Time-dependant evolution of the iron concentration of column effluent for a) all experimental duration and b) the first 50 days. The lines are not fitting functions, they simply connect points to facilitate visualization.

Figure 4: Influence of the Fe:pumice volumetric ratio on the removal efficiency of Cu^{II}, Ni^{II} and Zn^{II} as reflected by the Es (mg/g) values. The lines are not fitting functions, they simply connect points to facilitate visualization.

Figure 5: Magnitude of Cu, Fe, Ni and Zn release from the column with 10 % Fe^0. The lines are not fitting functions, they simply connect points to facilitate visualization.

Figure 6: (a) Comparison of the initial porosity and the specific efficiency (Es value for Zn) as influenced by the Fe:pumice volumetric ratio, (b) Time-dependant evolution of the hydraulic conductivity in all six systems. The lines are not fitting functions, they simply connect points to facilitate visualization.

Figure 7: (a) Time-dependant evolution of the residual porosity in all six systems and (b) residual porosity $\Phi(t)/\Phi_0$ for three values of the expansion coefficient η. The residual porosity is $\Phi(t)/\Phi_0 = 0$ for systems with clogging before Fe^0 depletion and $\Phi(t)/\Phi_0 \neq 0$ at Fe^0 depletion. The lines are not fitting functions, they simply connect points to facilitate visualization.

Supplementary Information: Material characterization

Improving the sustainability of granular iron/pumice systems for water treatment

Stefania Bilardi[a], Paolo S. Calabrò[a], Sabine Caré[b], Nicola Moraci[a], Chicgoua Noubactep[c,d,*]

[a]Università degli Studi Mediterranea di Reggio Calabria, MECMAT, Mechanics and Materials Department, Faculty of Engineering, Via Graziella, loc. Feo di Vito, 89122 Reggio Calabria, Italy.

[b]Université Paris-Est, Laboratoire Navier (UMR 8205), CNRS, ENPC, IFSTTAR, F-77455 Marne-la-Vallée, France

[c]Angewandte Geologie, Universität Göttingen, Goldschmidtstraße 3, D-37077, Göttingen, Germany.

[d]Kultur und Nachhaltige Entwicklung CDD e.V., Postfach 1502, D-37005 Göttingen, Germany

* e-mail: cnoubac@gwdg.de; Tel. +49 551 39 3191, Fax. +49 551 399379.

Content

SI1 Material characterization

Table SI1: Composition and experimental duration of the studied columns.

Table SI2: Characteristics of Fe^0 and pumice particles tested by MIP.

Figure SI1: SEM images of the Fe^0 and pumice particles.

Figure SI2 : Grain size distributions of Fe^0 and pumice.

Figure SI3: Cumulative volume intruded and pore size distribution of the pumice particles.

* Corresponding author: Tel. +49 551 39 3191, Fax. +49 551 399379; E-mail: cnoubac@gwdg.de.

SI Material characterization

SI1 Experimental Section

The microstructure of used Fe^0 and pumice was characterized using mercury intrusion porosimetry (MIP) measurements and by scanning electron microscopy (SEM) observations.

Moreover grain size distribution and the geotechnical parameters (i.e. coefficient of uniformity and mean grain size) derived from it have been determined.

SI1.1 MIP

MIP is performed by injecting mercury into a desaturated porous material. The in-pore invasion process is supposed to be governed by the Washburn-Laplace equation in which the size of intruded pore accessed, assimilated to cylindrical pores are inversely proportional to the applied pressure according to Eq. 5 (Washburn, 1921):

$$P = -\frac{2\gamma\cos\theta}{R_p} \qquad \text{(SI1)}$$

where P is the mercury injection pressure (Pa), γ is the surface tension of mercury (0.485 N/m), θ is the contact angle between solid and mercury ($\theta = 130°$) and R_p is the pore access radius for cylindrical pores (m). MIP measurements have been carried out using a Micromeritics instrument apparatus type (AutoPore IV 9500). The instrument is capable of a minimum intruding pressure of 3.4 kPa and a maximum pressure of 227 MPa, so that the pore radius ranges from 2.7 nm to 180 μm.

For pumice particles the measured pore data allow determining the inter-particular and intra-particular porosities of the pumice particles, the apparent specific weight ρ_{as} (defined as the ratio of the mass and the apparent volume of the pumice particles) and the specific weight ρ_s (defined as the ratio of the mass and the volume of the solid phase of the pumice particles).

SI1.2 SEM

During SEM (Hitachi, type: s3400N) observations, secondary electron mode was used. Pumice particles were coated with carbon. The observations enable a characterization of the morphology of both materials and of the inner pore structure of pumice.

SI2 Results and Discussion

SI2.1 SEM Observations of Fe^0 and pumice particles

SEM images detailing the microstructures of, respectively, Fe^0 and pumice particles are shown in Fig. SI1. These observations show that the Fe^0 and pumice particles are irregular. It can be observed that the pumice particles (grains) are porous with oval shaped and fibrous cavities (or pores). The diameter of these cavities at the surface is lower than about 40 μm (radius 20 μm).

SI2.2 MIP measurements of pumice particles

As shown in Fig. SI2, where for graphical convenience the pore size distribution is as usual expressed as $\frac{dV_i}{d(\log r)}(\log r)$ where V_i is the volume intruded by mercury and R is the pore equivalent radius, pumice exhibits a well defined peak around 70 μm and pores with equivalent radius inferior to 20 μm. According to the SEM observations, these results show that the pores with radius inferior to 20 μm can be attributed to the inner porosity of the pumice particles, so that the pores with equivalent radius superior to 20 μm can be attributed to the inter-particular porosity. The total porosity of the pumice medium Φ_0 (%)in the conditions used in MIP tests, is defined as:

$$\Phi_0 = V_{\text{mercury intruded}} * M / V \qquad \text{(SI3)}$$

Where $V_{\text{mercury intruded}}$ is the total intrusion volume (mL/g), M the mass of pumice (g) and V the volume of the pumice medium (mL).

The volume of the inter-particular volume Φ_{inter} (%) is given by:

$$\Phi_{\text{inter}} = V_{R>20\mu m} / V \qquad \text{(SI4)}$$

Where $V_{R>20\mu m}$ (mL) is the volume of intruded mercury in pores with radius superior to 20 μm.

It can be noticed that the compactness C_{pumice} (-) of the pumice particles, defined as the ratio of the apparent volume of the particles to the total packing volume (V = volume of the medium), is given by:

$$C_{pumice} = 1 - \Phi_{inter}. \qquad \text{(SI5)}$$

Furthermore, the volume of the intra-particular φ_{pp} is given by:

$$\varphi_{pp=} = V_{R<40\mu m} / V / C_{pumice} \qquad \text{(SI6)}$$

Where $V_{R<20\mu m}$ (mL) is the volume of intruded mercury in pores with radius inferior to 20 μm.

The results are given in Tab. SI2. The total porosity of the pumice medium has been estimated to be 73.3 % and the inner porosity of the pumice to be 41.0 %.

SI2.3 Grain size distributions of Fe^0 and pumice particles

The grain size distributions of Fe^0 and pumice particles are shown in Fig. SI3.

The main geotechnical parameters derived by the grain size distributions are the coefficient of uniformity U= d_{60}/d_{10} (i.e. ratio between the diameters corresponding to 60 and 10 % finer in the grain size distribution) and the mean grain size d_{50}(i.e. the diameters corresponding to 50 % finer in the grain size distribution).

The mean grain size (d_{50}) is about 0.5 mm and 0.3 mm for ZVI and Pumice respectively, their coefficients of uniformity (U) are, respectively 2 and 1.4 and therefore both materials are characterised by a uniform grain size distribution.

SI2.4 Porosity of the columns

Under the hypothesis that the relative density (packing) of granular mixtures are the same in the columns and in the MIP tests, the estimated porosity of the reactive zone can be given for systems A through E (Tab. 1, main text) according to:

$$\Phi_0 = \Phi_{inter} + \varphi_{pp} . f_{pp} \qquad \text{(SI7)}$$

where f_{pp} (-) is the pumice particle volume fraction determined by $f_{pp} = V_{pp}/V$ with V_{pp} the volume of the pumice particles and the V the volume of the reactive zone.

References

Washburn E.W., 1921. The dynamics of capillary flow, Phys. Rev. 17, 273–283.

Table SI1: Composition and experimental duration of the studied columns. *-marked systems were stopped because of excessive permeability loss.

System	Composition (Fe^0:pumice)	Duration (day)
A	0:100	45
B	10:90	90
C	25:75	36*
D	50:50	28*
E	75:25	22*
F	100:0	17*

Table SI2: Characteristics of Fe^0 and pumice particles tested by MIP.

	Fe^0	Pumice
Specific weight ρ_s (g/cm^3)	7.78	1.92
Apparent specific weight ρ_{as} (g/cm^3)	7.78	1.14
Compactness C (-)	0.51	0.45
Inter particular porosity Φ_{inter} (%)	49.6	54.8
Intra particular porosity φ_{pp} (%)	-	41.0
Porosity Φ_0 (%)	49.6	73.3

Figure SI1: SEM images of the Fe^0 particles (A) and of the pumice particles (B).

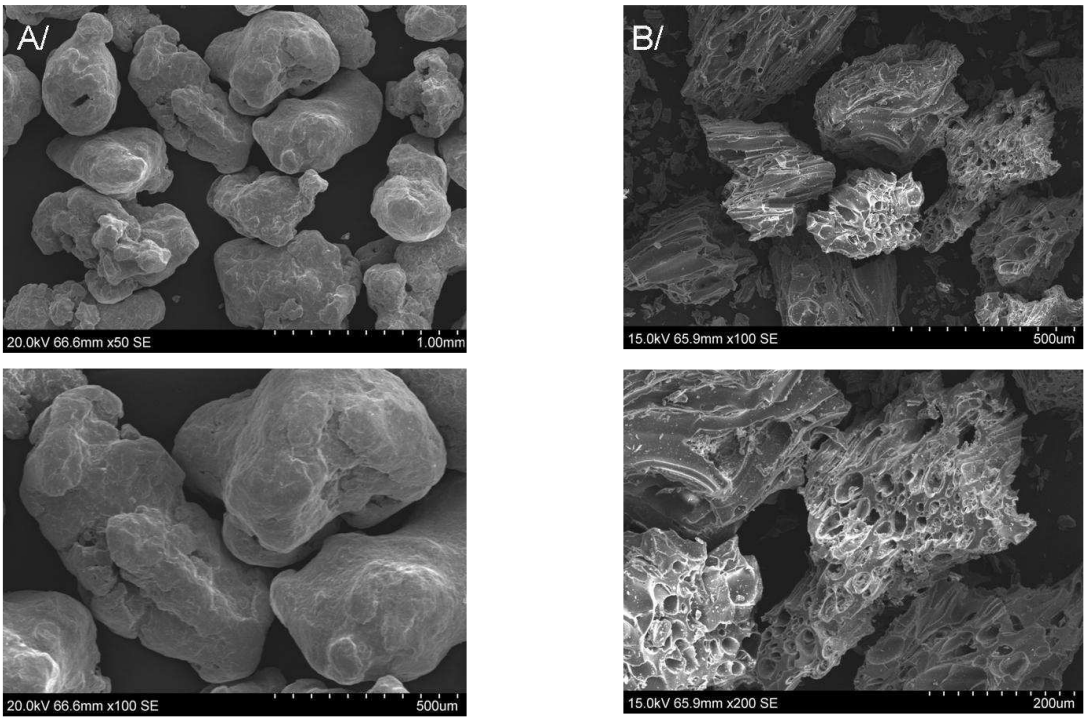

Figure SI2: Cumulative volume intruded (mL/g) and pore size distribution of the pumice particles. Two types of porosity are observed: inter particular porosity Φ_{inter} (R > 20μm) and intra particular porosity φ_{pp} (R < 20μm).

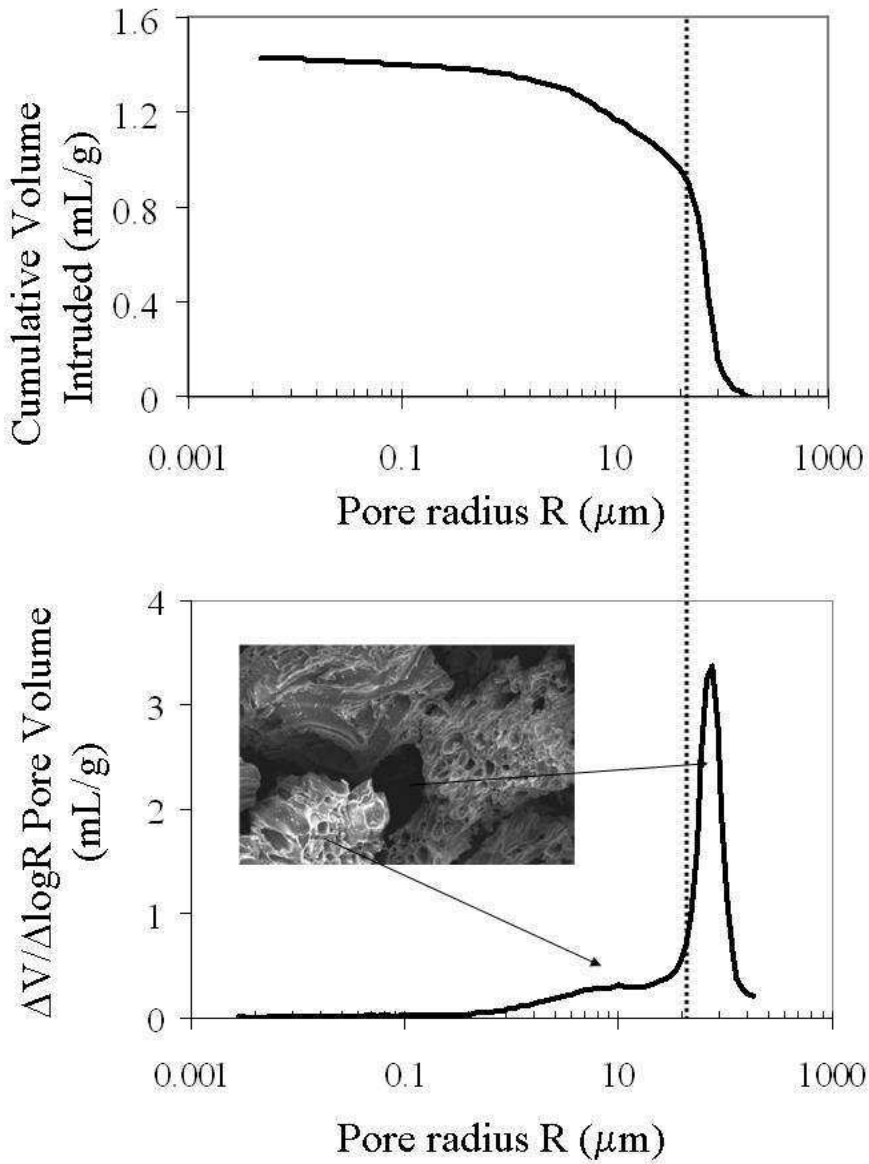
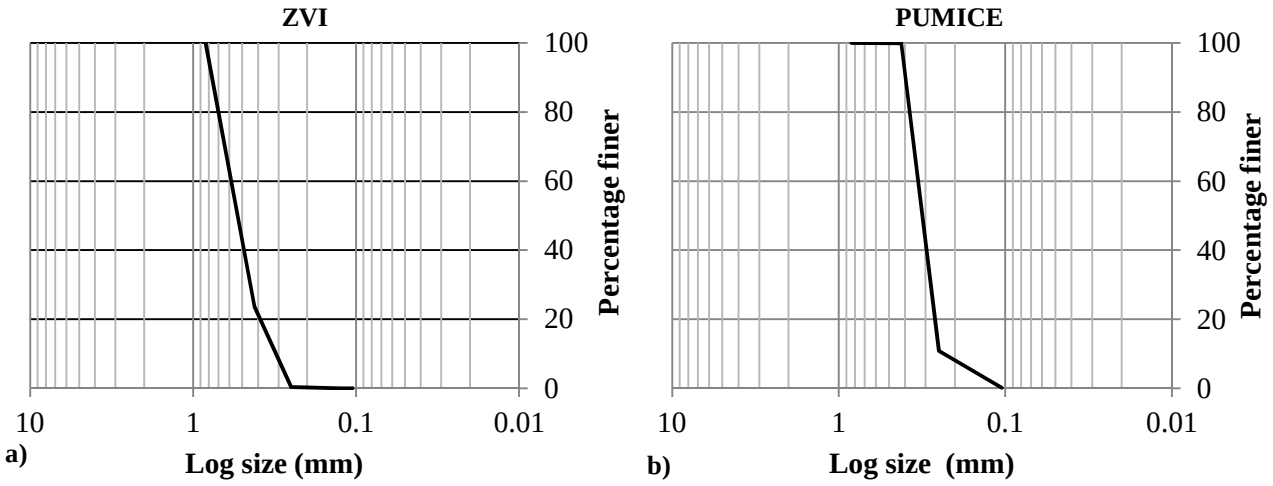
Figure SI3: Grain size distributions of used materials: Fe^0 (a) and pumice (b).